

# Drop Behaviour on Micro-Structure SuperHydrophobic Coating

Ramin Kamali Moghadam<sup>1\*</sup>, Mohammad Taeibi Rahni<sup>2</sup>, Salar Heyat Davoudian<sup>3</sup> and Reinhard Miller<sup>4</sup>

1. Aerospace Research Institute, Ministry of Science, Research and Technology, Tehran, Iran
- 2, 3. Department of Aerospace Engineering, Sharif University of Technology, Tehran, Iran
4. Max Planck Institute of Colloids and Interfaces, D-14424 Potsdam, Germany

\*Corresponding Author's E-mail: [rkamali@ari.ac.ir](mailto:rkamali@ari.ac.ir)

## Abstract

Superhydrophobic coatings can be made by creating a micro-sized structure on a surface providing super-repellent properties which have many applications in aerospace, defense, automotive, biomedical and engineering. Numerical simulation of drop dynamics and motion on a superhydrophobic surface helps us understand control and building surface textures and find optimum micro structured coatings of the maximum hydrophobicity. In the present work, the dynamics of drops on superhydrophobic inclined micro-structured surfaces is studied, using a finite element method. Effects of microstructures on droplet behavior on a superhydrophobic surface is investigated using different microstructures. The governing equations and important dimensionless numbers are described and a numerical algorithm is introduced. The validation of the numerical algorithm is performed by simulation of drop motion attached to an inclined surface. In addition, droplet movement on the micro structured surface is numerically simulated on smooth and microstructure surfaces in the same conditions. Comparison of the results shows the effect of microstructure coating on the surface hydrophobicity properties.

**Keywords:** Micro-Structured, Superhydrophobic surfaces, Numerical simulation, Drop motion

## Nomenclature

$r$	the roughness factor
$f_1$	the fractions of the liquid-solid
$f_2$	liquid-air interfaces
$f_2$	liquid-air
$\rho_D$	density
$\mu_D$	viscosity of the droplet
$\sigma$	surface tension coefficient
$R$	radius of a circular droplet
$V^*$	dimensionless velocity
$t^*$	time
$C_D$	drag coefficient

variety of material surfaces so that they exhibit non-wetting properties. Many diverse applications have been found in the fields, such as space and aerospace, defence, automotive, biomedical applications and engineering, sensors, apparels, and so on [1-5]. Superhydrophobic surfaces repel water generally due to their surface texture or chemical properties.

The behavior of water droplets on a surface can be related to surface energies and wettability. When the surface energy of the materials is low, the molecules in the water droplets are more attracted to each other as compared with hydrophobic surface having a higher contact angle. The basis of hydrophobicity is the creation of recessed areas on a surface whose wetting expends more energy than bridging the recesses expends. Instead of using basic atoms for repellence like many successful hydrophobic penetrating sealers, superhydrophobic products are coatings which

## Introduction

Over the years, researchers have been working to mimic the nature by inducing superhydrophobic properties into a

1. Associate Professor  
2. Professor

3. Ph.D. Student  
4. Professor



### COPYRIGHTS

© 2022 by the authors. Published by Aerospace Research Institute. This article is an open access article distributed under the terms and conditions of [the Creative Commons Attribution 4.0 International \(CC BY 4.0\)](https://creativecommons.org/licenses/by/4.0/).

### How to cite this article:

R. Kamali Moghadam, M. Taeibi Rahni, S. Heyat Davoudian and R. Miller, "Drop Behavior on Micro-Structure Super Hydrophobic Coating," *Journal of Space Science and Technology*, Vol. 15, Special Issue, pp. 25-33, 2022, <https://doi.org/10.30699/jsst.2020.1241>.

create a micro/nano-sized structure on a surface providing super-repellent properties [5-7].

The coating causes an almost imperceptibly thin layer of air to form on the surface. Superhydrophobic surfaces (SHS) can be used in building materials, such as glass, ceramics, and concrete, for keeping buildings clean. In addition, they have important applications in maritime industry, e.g., they can yield skin friction drag reduction for ships' hulls. Also, superhydrophobic coatings have potential uses in vehicle windshields to prevent disturbing rain droplets. The coatings help to remove salt deposits from unclean water. They are also applicable for producing passive anti-icing surfaces. The anti-icing properties of superhydrophobic materials (including delayed frosting, ice-adhesion reduction, snow-adhesion reduction and delayed water drop freezing) are more complex to understand, due to various factors involved, for example surface chemistry, roughness, and environmental condition [8-10]. Hydrophobicity can also affect the droplet/bubble velocity, and it was shown that bubbles attached to a hydrophobic surface have a rising velocity even higher than that of free rising bubble [11].

With a combination of surface chemical and roughness modifications in superhydrophobic materials, water drops on a SHS show a large contact angle (CA) and a small CA hysteresis. On a smooth surface, the contact angle of a water droplet can be increased to only  $120^\circ$  by lowering the surface free energy [12]. The construction of micro/nano-structures on a smooth surface can lead to contact angles of water drops of up to  $150^\circ$ . Thus, SHS are well-known for their excellent water-shedding and self-cleaning properties. Numerical simulation of drop dynamics and motion on a superhydrophobic surface helps us understand how to control and build surface textures and find optimum micro/nano-structured coatings of maximum hydrophobicity [13].

In the present work, dynamics of droplets on superhydrophobic inclined micro structured surfaces is studied using numerical simulations. The governing equations and important dimensionless numbers are described and the numerical algorithm is explained. All simulations are performed by COMSOL Multiphysics 5.2 and finite element method. The validation of the numerical algorithm is performed by simulation of the droplet movement attached to an inclined surface. Moreover, the droplet movement on the micro-structured surface is simulated to capture the effect of micro-structured coatings on the surface hydrophobicity. Also, the effects of microstructures on droplet behaviour in rest on a superhydrophobic surface is investigated using five new microstructures. It is noted that droplet dynamics on different microstructures have been studied before by the authors [14].

### Problem Description

The gravitational driven movement of 2D droplets attached to an inclined superhydrophobic wall is studied here. Figure

1 shows the schematics of the problem at its initial condition where a semi-circular droplet is initially at rest and attached to an inclined wall to a quiescent air phase. As demonstrated in the figure, the initial contact angle of all attached drops is  $90^\circ$ ; however, during the solution depending on the wettability of the wall, the contact angle changes to its real values (e.g.  $120^\circ$  for the hydrophobic surface). The surface has a roughness on a micro-scale; there are air pockets so we deal with the Cassie regime for the droplet. The initial pressure of the domain is set to be 1 atm. Accordingly, all droplets are initially at rest and get started to move immediately due to the gravity forces for  $t > 0$ .

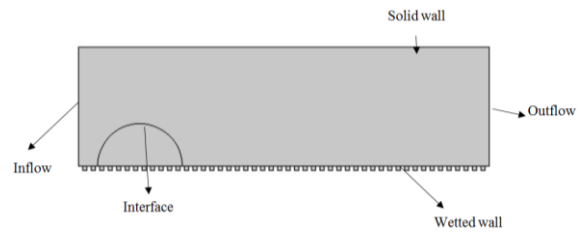


Fig. 1: Schematics of the physical domain

For a rough surface, two wetting states may occur if a droplet is deposited on the surface: the non-composite/Wenzel state (i.e., complete liquid penetration into the grooves of a rough surface) and the composite/Cassie state (i.e., the entrapment of air in the grooves of a rough surface), (see Fig.2) [15].

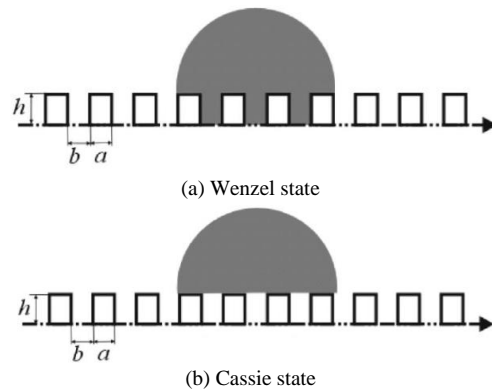


Fig. 2: Wenzel/Cassie state on a uniformly rough surface [15]

Note that the surface micro-texture is uniformly constructed from the constant geometrical parameters of pillar width ( $a$ ), spacing ( $b$ ), and height ( $h$ ) and the length scale of the posts is much smaller than the droplet size. The apparent CA of the non-composite is given by Wenzel's equation

$$\cos(\theta^*) = r \cos \theta \quad (1)$$

where  $r$  is the roughness factor as the ratio between the actual area and the geometric projected area for a wetting surface; for the 2D model,  $r = 1 + 2h/(a + b)$ . However, the apparent CA of the composite,  $\theta_{CB}$ , can be calculated using the Cassie-Baxter equation:

$$\cos(\theta_{CB}) = f_1 \cos \theta_1 + f_2 \cos \theta_2 \quad (2)$$

where  $f_1$  and  $f_2$  are the fractions of the liquid-solid and liquid-air interfaces with intrinsic equilibrium contact angles  $\theta_1$  and  $\theta_2$ , respectively. For one aqueous droplet on the rough surface,  $\theta_1$  equals the intrinsic CA ( $\theta$ ) and  $\theta_2$  equals  $180^\circ$ , leading to a changed form of the Cassie-Baxter equation:

$$\cos(\theta_{CB}) = f \cos \theta - (1 - f) \quad (3)$$

where  $f$  is the solid-liquid contact area fraction of the substrate; for the 2D model,  $f = a/(a + b)$ . The most important dimensionless numbers in this field are the Reynolds and Bond numbers:

$$\text{Re} = \frac{\rho_D \sigma R}{\mu_D^2}, \quad \text{Bo} = \frac{\rho_D g R^2}{\sigma} \quad (4)$$

where  $\rho_D$  and  $\mu_D$  are the density and viscosity of the droplet, respectively, and  $\sigma$  is the surface tension coefficient. Also,  $R$  is the radius of a circular droplet and is considered such that the volume of the droplet attached to the wall and the droplet moving free in the domain are the same. The other important dimensionless parameters are density ratio  $\rho^* = \rho_D/\rho_A$  and viscosity ratio  $\mu^* = \mu_D/\mu_A$  where  $\rho_A$  and  $\mu_A$  are the density and viscosity of air, respectively. The dimensionless velocity ( $V^*$ ), time ( $t^*$ ), and drag coefficient ( $C_D$ ) are defined as follows:

$$V = \frac{V_D}{V_\infty}, \quad t = \frac{t^* \sigma}{\rho V}, \quad C_D = \frac{D}{0.5 \rho V_\infty^2 A} \quad (5)$$

where in  $D$ ,  $A$ ,  $V_D$ , and  $V$  represent the drag force, droplet surface, droplet moving velocity, and droplet volume, respectively.  $V_\infty$  is calculated using the ratio of the surface tension to the liquid viscosity,  $V_\infty = \frac{\sigma}{\mu_D} = \text{const}$ .

The results obtained in this study are discussed based on these dimensionless parameters.

## Governing Equations

The equations governing the motion of the two fluids are the modified Navier–Stokes equations:

$$\rho \left( \frac{\partial \mathbf{u}}{\partial t} + \mathbf{u} \cdot \nabla \mathbf{u} \right) = -\nabla p + \nabla \cdot [\mu (\nabla \mathbf{u} + \nabla \mathbf{u}^T)] + \mathbf{SF} + \rho \mathbf{g} \quad (6)$$

$$\nabla \cdot \mathbf{u} = 0 \quad (7)$$

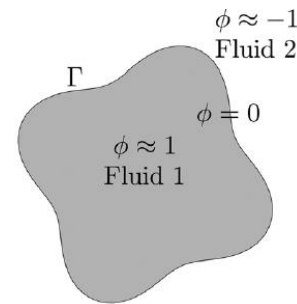
where  $\mathbf{u}(\mathbf{x}, t)$  is the velocity,  $p(\mathbf{x}, t)$  is the pressure,  $\rho(\mathbf{x}, t)$  is the density, and  $\mu(\mathbf{x}, t)$  is the viscosity which are dependent on time,  $t$ , and on the Cartesian coordinate vector,  $\mathbf{x}(x, y)$ .  $\mathbf{g}$  is the gravitational force vector, and the superscript  $T$  denotes the transpose. The continuum surface force (CSF) model is used to represent the singular surface tension force,  $\mathbf{SF}$ :

$$\mathbf{SF} = -\sigma \kappa \delta_\Gamma \mathbf{n} \quad (8)$$

where  $\kappa$  is the mean curvature of the interface,  $\delta_\Gamma$  is the surface  $\delta$  function, and  $\mathbf{n}$  is the unit normal vector to the interface directed from fluid 1 to fluid 2.

To solve the droplet movement on a superhydrophobic surface, the phase-field method (PFM) is used. PFM is an increasingly popular method for modeling the dynamics of multiphase fluids.

Several numerical methods have been developed for interfacial flows. These methods are generally classified into three groups: 1) Interface tracking methods (ITM) like ALE and MAC [16, 17], 2) Interface capturing methods (ICM) such as VOF, Level Set, Phase Field [18, 19], and 3) Meshless methods including LBM and SPH [20]. The ITMs require the meshes to track the interfaces. However, in the ICMs, the computations are based on fixed spatial domains, where an interface function, marking the location of the interface, is computed to capture the interface. In these methods, the interface is captured within the resolution of the finite element mesh covering the area where the interface is. In some cases, like the present problem, the interface might be too complex to track and then the application of ITMs is no longer feasible. The main drawback of the VOF (Volume of Fluid) is that it's smearing of interface. For problems which surface tension is dominant, this could cause problems. To overcome this drawback and to have a better interface capturing, the VOF should be coupled with the phase field method which has problem in satisfying conservation properties. In the PFM, there is a diffuse-interface with a finite width between two phases. The density, the viscosity, and other physical quantities are characterized by an order parameter, which is governed by the modified Cahn–Hilliard equation. This equation was firstly proposed by Cahn and Hilliard to describe the initial stage of spinodal decomposition [21]. It models the interface dynamics, including the surface minimization, the topological changes, and the phase separation [21]. In this method, two fluid phases are separated by a thin interface and are determined using a parameter of  $\phi$  by measurement of their volume fraction as shown in Fig. 3. Fluid 1 and 2 are defined by  $\phi \approx 1$  and  $\phi \approx -1$ , respectively, and the interface  $\Gamma$  is determined by  $\phi = 0$ .



**Fig. 3:** General definition of the Phase-Field Method (PFM) [21]

The evolution of the phase-field function  $\phi$  is governed by the advective Cahn–Hilliard equation as follows [21]:

$$\frac{\partial \phi}{\partial x} + \nabla \cdot (\phi \mathbf{u}) = M \Delta \lambda \quad (9)$$

where  $M$  is the constant mobility and  $\lambda$  is the chemical potential computed as:

$$\lambda = F'(\phi)^2 - \varepsilon^2 \Delta \phi \quad (10)$$

$F(\phi) = (1 - \phi^2)^2/4$  is the bulk energy density which has two minima corresponding to the two stable phases of the fluid, and  $\varepsilon$  is a measure for the interface thickness. It is

convenient to use the dimensionless Peclet number, which is defined as  $Pe = U_c L_c / M$ , where  $U_c$  is the characteristic velocity and  $L_c$  is the characteristic length. This non-dimensional parameter allows that the PFM can be applied to many physical phase states such as miscible, immiscible, and partially miscible ones. However, the phase-field function quickly changes near the interface and, hence, must be well resolved. In other words, a relatively large number of grid points near the interface is needed. Choosing an appropriate value of  $\varepsilon$  is important for the accuracy of calculations. Too large values of  $\varepsilon$  can make nonphysical solutions, while too small ones lead to numerical difficulties.

All simulations are performed by COMSOL Multiphysics 5.2. The fully coupled finite element method and PARDISO solver which is the nonlinear Newtonian method are used for simulations. Pre ordering method is selected as "Nested dissection multi-threaded". Damping factor is set as 1 and Jacobean update is performed once per time step. For the phase field setup, the controlling interface thickness,  $\varepsilon_{pf}$ , is selected as  $h_{max}/2$ , where  $h_{max}$  is the maximum mesh size on the interface. Also, the mobility tuning is considered as unit in present simulations.

## Boundary Conditions

Different types of boundary conditions are considered in the present solution. According to figure 1, the left boundary is considered as zero-velocity boundary (Inflow) and the right one is considered to be at ambient pressure (Outflow). The top boundary is set as no-slip solid wall and the wetted wall feature is selected for solid walls in contact with a fluid interface. It sets zero for the normal velocity component

$$\mathbf{u} \cdot \mathbf{n}_{wall} = 0 \quad (11)$$

and adds a frictional boundary force,  $\mathbf{F}_{fr}$ , as

$$\mathbf{F}_{fr} = -\frac{\mu_D}{\beta} \mathbf{u} \quad (12)$$

Here,  $\beta$  is the slip length,  $\mathbf{n}_{wall}$  is the normal vector to the wall and  $\mathbf{u}$  is the velocity vector of the liquid. Using this type of boundary condition, the contact angle, the angle between the wall and the fluid interface, can be specified. Furthermore, PFM is used to define the interface between drop and air.

Obviously, the droplet dynamics contact angle (CA) with a wall surface is the most important parameter for drop motion on solid surface. The equilibrium CA, which shows the balance of energy release and small-scale dissipation, is calculated by the Young relation [14]:

$$\sigma_{sl} + \sigma \cos \theta_e = \sigma_{sg} \quad (13)$$

At dynamic conditions, the CA is assumed to be locally calculated by the Young relation (Eq. (13)). However, during drop motion on the surface, the Eq.

(13) is not necessarily valid. In dynamic condition, the CA hysteresis expression is defined as the difference between the advancing and receding angles [22]. Determination of the dynamic CA is very sensitive and different relations are used to determine it more accurately both theoretically and even empirically [22]. Dynamic contact angle models, including hydrodynamic models, molecular kinetic models, experimental models, as well as hybrid models are developed to obtain accurate contact angle and meniscus displacement [14]. Most of these models give the relationship between the contact line velocity and the dynamic contact angle. This form is known as the hydrodynamic model whose resulting formula describes the change in the dynamic contact angle due to viscous bending of the liquid-gas interface.

## Validation

### Freely Falling Droplet

Drops in free fall in infinite media under the influence of gravity are generally grouped under the following three categories [23]:

1. Spherical: Generally speaking, drops are closely approximated by spheres if interfacial tension and/or viscous forces are much more important than inertia forces.
2. Ellipsoidal: The term "ellipsoidal" is generally used to refer to drops which are oblate with a convex interface (viewed from inside) around the entire surface.
3. Spherical-cap or ellipsoidal-cap: Large drops tend to adopt flat or indented bases and to lack any semblance of fore-and-aft symmetry.

Such fluid particles may look very similar to segments cut from spheres or from oblate spheroids of low eccentricity; in these cases, the terms "spherical-cap" and "ellipsoidal-cap" are used. If the fluid particle has an indentation at the rear, it is often said to be "dimpled." Large spherical- or ellipsoidal-caps may also trail thin envelopes of dispersed fluid referred to as "skirts." For bubbles and drops rising or falling freely in infinite media it is possible to prepare a generalized graphical correlation in terms of the Eotvos number,  $Eo$ , Morton number,  $M$ , and Reynolds number,  $Re$ . [23]. Note that Fig. 8 does not apply to the extreme values of density ratio or viscosity ratio found for liquid drops falling through gases.

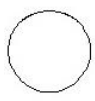

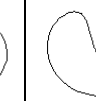
$$Eo = \frac{g \Delta \rho d_d^2}{\sigma}, \quad M = \frac{g \mu^4 \Delta \rho}{\rho^2 \sigma^3}, \quad Re = \frac{\rho d_e U}{\mu} \quad (14)$$

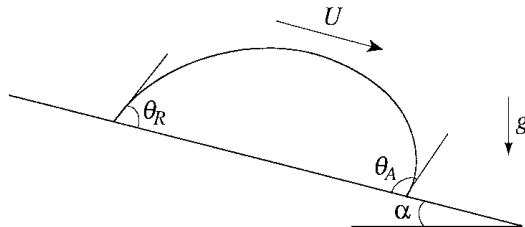
In this study, to validate the simulation, three cases are simulated at certain conditions according to table 1. The results show that the captured shapes in the present simulation and mentioned conditions are consistent to those in Ref. [23].

### The Droplet Attached to an Inclined Surface

Here, a drop will be considered whose mass center moves with a steady velocity  $U$  down a plane inclined at the angle  $\alpha$  with respect to the horizontal line, as shown in Fig. 4. It is first necessary to determine which parameters affect the drop sliding velocity in order to achieve meaningful experimental measurements. To this end, a dimensional analysis has been performed to obtain the functional dependency of similar variables relevant to the system. The drop has a radius  $R_0$  when in a spherical shape. It is assumed that  $U$  is dependent on  $R_0$ ,  $\sigma_D$ ,  $\mu_D$ , the gravitational force per volume,  $\rho g \sin \alpha$ , and on interfacial parameters. The interfacial parameters include the microscopic length scale,  $\lambda$ , which relieves the classical no-slip boundary condition at the contact line, and the static and dynamic contact angles. It is noted that different theories on the contact line dynamics may choose different sets of interfacial parameters.

**Table 1:** The predicted droplet shapes as a function of Reynolds and Bond numbers. The ratios of density and viscosity are set to be  $\frac{\rho_{Drop}}{\rho_{Air}} = 10$  and  $\frac{\mu_{Drop}}{\mu_{Air}} = 1$ , respectively.

Parameters	Eo = 200 M = 10	Eo = 5 M = 0.0001	Eo = 1 M = 0.01
Drop shape			



**Fig. 4:** Shape of a drop sliding down an inclined surface [24].

The fluid properties are shown in Table 2 with their capillary length  $\kappa^{-1}$ .

**Table 2:** Physical properties of the liquids used in the simulation [24]

Liquid	EG (Ethylene Glycol)	GW (Glycerin-Water)	Glycerin
Density (kg/m <sup>3</sup> )	1114	1228	1260
Viscosity (Pa · s)	0.0209	0.0600	0.95
Surface Tension (N/m)	0.0484	0.0641	0.063
$\kappa^{-1}$ (mm)	2.1	2.3	2.3
(°) $\theta_e$	70.2	73.6	78.1

To validate the simulation, the obtained numerical results have been compared to experimental data in Table 3. Note, the present algorithm can cover the empirical droplet velocity with a maximum error of 2.46%.

**Table 3:** Comparison of results of the present solution and experimental data

Liquid	Volume (mm <sup>3</sup> )	$\alpha$ (°)	$U$ ( $\frac{mm}{s}$ ) [23]	$U$ ( $\frac{mm}{s}$ ) (Present)	Error (%)
EG	15.1	14	0.229	0.234	2.18
GW	24.0	20	0.122	0.125	2.46
Glycerin	77.8	14	0.041	0.0419	2.19

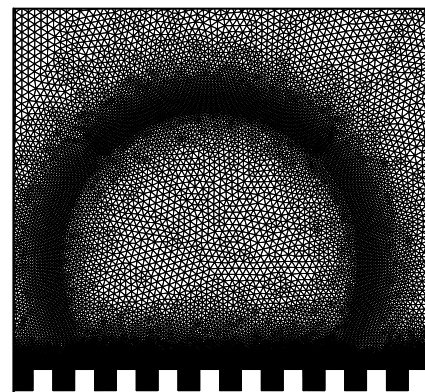
## Results and Discussions

### Droplet on a Superhydrophobic Surface

In this study, the Cassie state on a rough surface and its effect on the contact angle are investigated. Firstly, the water drop on a hydrophobic surface has been numerically simulated and the results are shown in Fig. 5. The initial contact angle is 0° and the equilibrium condition is obtained at  $t = 1$  with the contact angle of 120°.

To investigate the effects of the micro-structured surfaces on the equilibrium contact angle, another simulation of the drop placed on the micro-roughness elements has been performed with the same initial conditions. Dimension of the microstructured roughness is  $a = b = 0.1 \text{ mm}$ . As shown in Fig. 6, the droplet does not impregnate the rough solid, leaving a trapped vapor layer. From Eq. (3), the Cassie-Baxter contact angle should be 138.6° and in the present simulation, it is calculated about 136.9°, and so there is a good agreement between the simulated result and the analytical solution.

For complex two-phase flows, choosing a proper mesh is very important, in particular when there is a sharp interface. Therefore, mesh treatment plays a crucial role in stability, convergence, and accuracy of the numerical solution. In the present study, the phase field scheme is used to precisely capture the interface when the droplet is moving. Fig. 4 shows the meshes, generated for the droplet and air at the initial position of the drop. About 100,000 unstructured cells with concentration at the droplet interface have been used in all solutions. For more accurate simulation of droplet, mesh refinement method near droplet boundary has been used. It is noted that the grid study and the solution independency have been performed for the solutions.



**Fig. 4:** Generated mesh around the drop on the microstructure surface



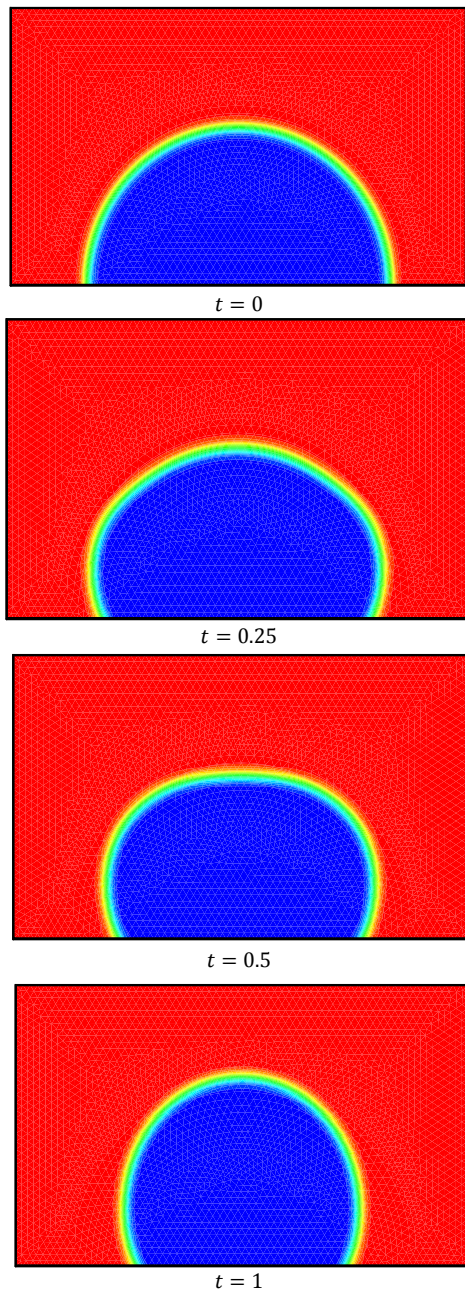


Fig. 5: Simulation of water droplet on a hydrophobic surface at different times

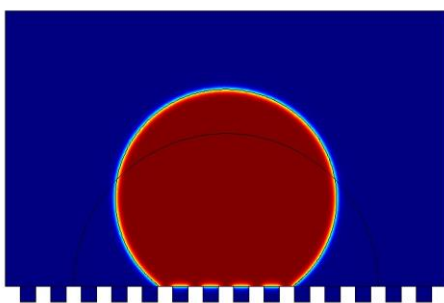


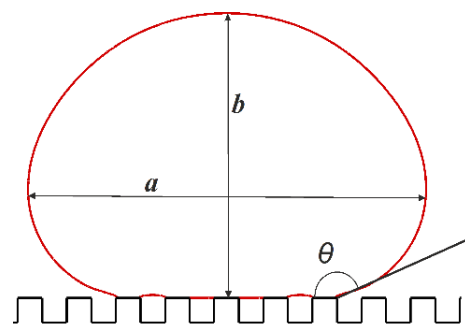
Fig. 6: Simulation of water droplet on a micro-structured superhydrophobic surface at equilibrium condition

### Effects of Microstructures on Droplet Behavior on a Superhydrophobic Surface

In this section, effect of microstructures on droplet behavior in rest on a superhydrophobic surface is studied. For this purpose,

five microstructures are selected as seen in Fig. 7 and the droplet behavior is simulated on them for different times. Dimensions of the micro-structures are in the same order and similar to that of the previous section. It is obvious that the structure of superhydrophobic surfaces has strong effect on the shape and the equilibrium contact angle of droplet at steady state condition. For more accurate studies, these two parameters are compared in table 2. The  $a$ ,  $b$ , and  $\Theta$  parameters, which determine droplet shape, are specified in table 4. It is indicated that the microstructure of case 1, makes more contact angle at 0.03 s for the droplet in rest. However, this behavior may be different for the droplet in motion. With the obtained results, effects of microstructures on droplet motion is investigated in the next section.

Table 4: Comparison of droplet shape on different microstructures



Case	$a/b$				$\Theta$ (deg)			
	0 (s)	0.01 (s)	0.02 (s)	0.03 (s)	0 (s)	0.01 (s)	0.02 (s)	0.03 (s)
1	2	1.4	1.38	1.1	90	150	145	137
2	2	1.39	1.37	1.06	90	147	145	130
3	2	1.4	1.2	1.14	90	143	140	135
4	2	1.42	1.38	1.03	90	148	145	130
5	2	1.4	1.33	1.06	90	155	147	132

### Droplet Motion on Hydrophobic and Superhydrophobic Surface

In this case, the droplet motion on both inclined smooth and micro-structured rough surfaces is studied. Here, the inclination angle is  $15^\circ$  and the contact angle is  $135^\circ$ . Dimension of the micro-textures is  $a = b = 0.05 \text{ mm}$ . The comparison of the droplet motion on smooth and micro-structured surfaces at different times, shown in figure 8, indicates that the droplet on the inclined micro-structured surface has more velocity than the smoothed one. The results show that the equilibrium contact angle for the micro-structured surface at different times is also about 26% larger than the same angle on the smoothed

one. This fact demonstrates the effect of the micro-structured surface with an increased hydrophobicity. To accurately investigate the results, a comparison of the position and the velocity of the drop on both inclined smooth and microstructure surfaces is presented in figure 9. It is found that the drop on the microstructure surface reaches the destination about 6% faster than on the smooth one with about 7% more velocity. It is noted that in the present simulation, the final time of the drop reaching the end of surface ( $x=8$  mm) is about 0.099 ms for the smoothed surface and 0.093 ms for the microstructure one.

### Conclusions

In the present work, a superhydrophobic surface has been proposed by creating a micro-sized structure. Numerical simulation is one of the efficient methods to investigate the performance of the superhydrophobic surface in the field of hydrophobicity. The main goal of the present study is to investigate the effects of microstructures on superhydrophobicity of the surfaces. For this purpose, simulation of droplet on different microstructures has been studied at droplet rest and comparison of the results is performed on the

smoothed surface as well. The dynamics of drops on the superhydrophobic inclined micro-structured surfaces has been studied using a finite element method. The governing equations have been described and a numerical algorithm has been introduced. The numerical algorithm has been validated by simulation of drop motion attached to an inclined surface in different conditions. Effects of microstructures on droplet behavior on a superhydrophobic surface in rest is investigated using five new microstructures. It is indicated that the microstructure of case 1, makes more contact angle for the droplet in rest. Moreover, droplet movement on the micro structured surface is numerically simulated on smooth and microstructure surfaces in the same conditions to capture the effect of micro-structured coatings on the surface hydrophobicity. The results indicate that the equilibrium contact angle for the micro-structured surface at different times is about 26% larger than on the smoothed one. This fact demonstrates the effect of the micro-structured surface with an increased hydrophobicity. It is also found that the drop on the microstructure surface reaches the destination about 6% faster than on the smooth one with about 7% more velocity.

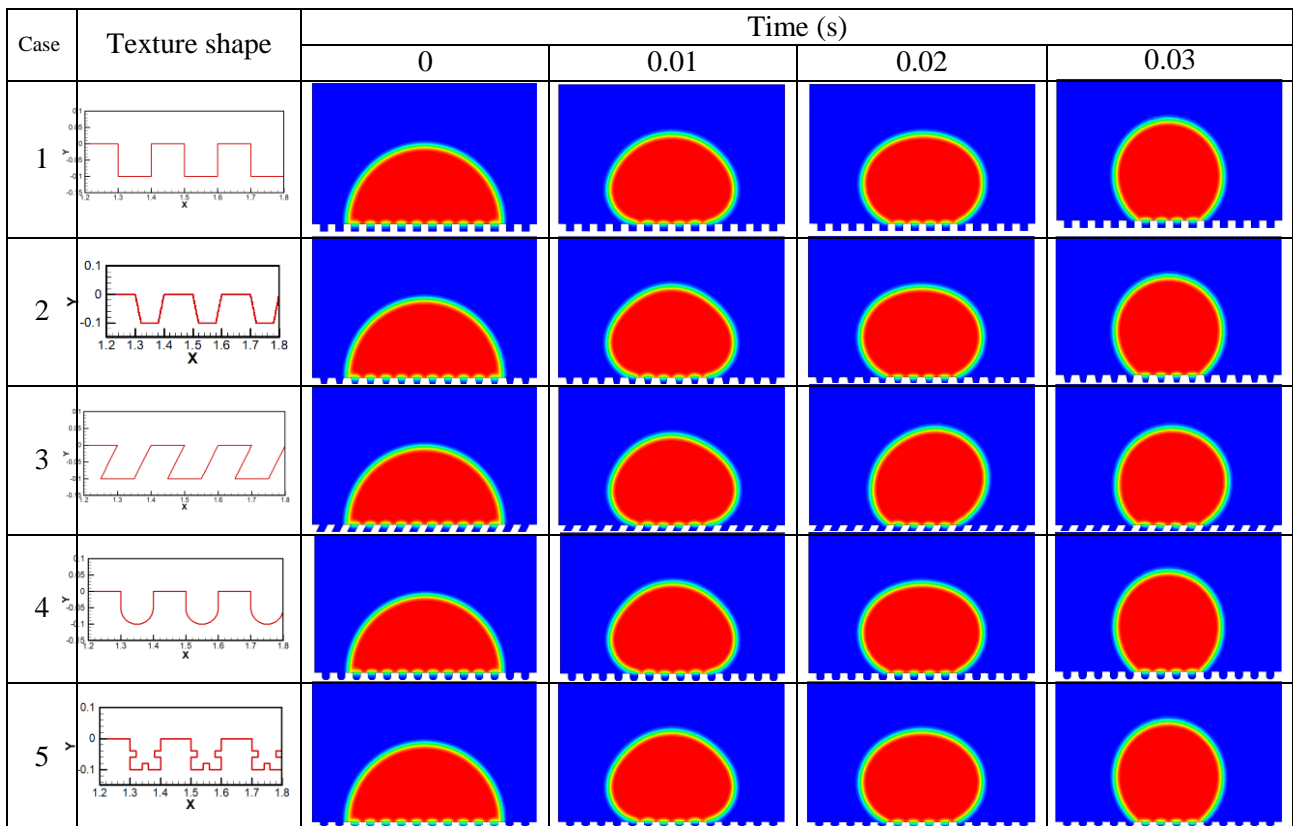


Fig 7: Effect of different microstructures on droplet behavior on a superhydrophobic surface

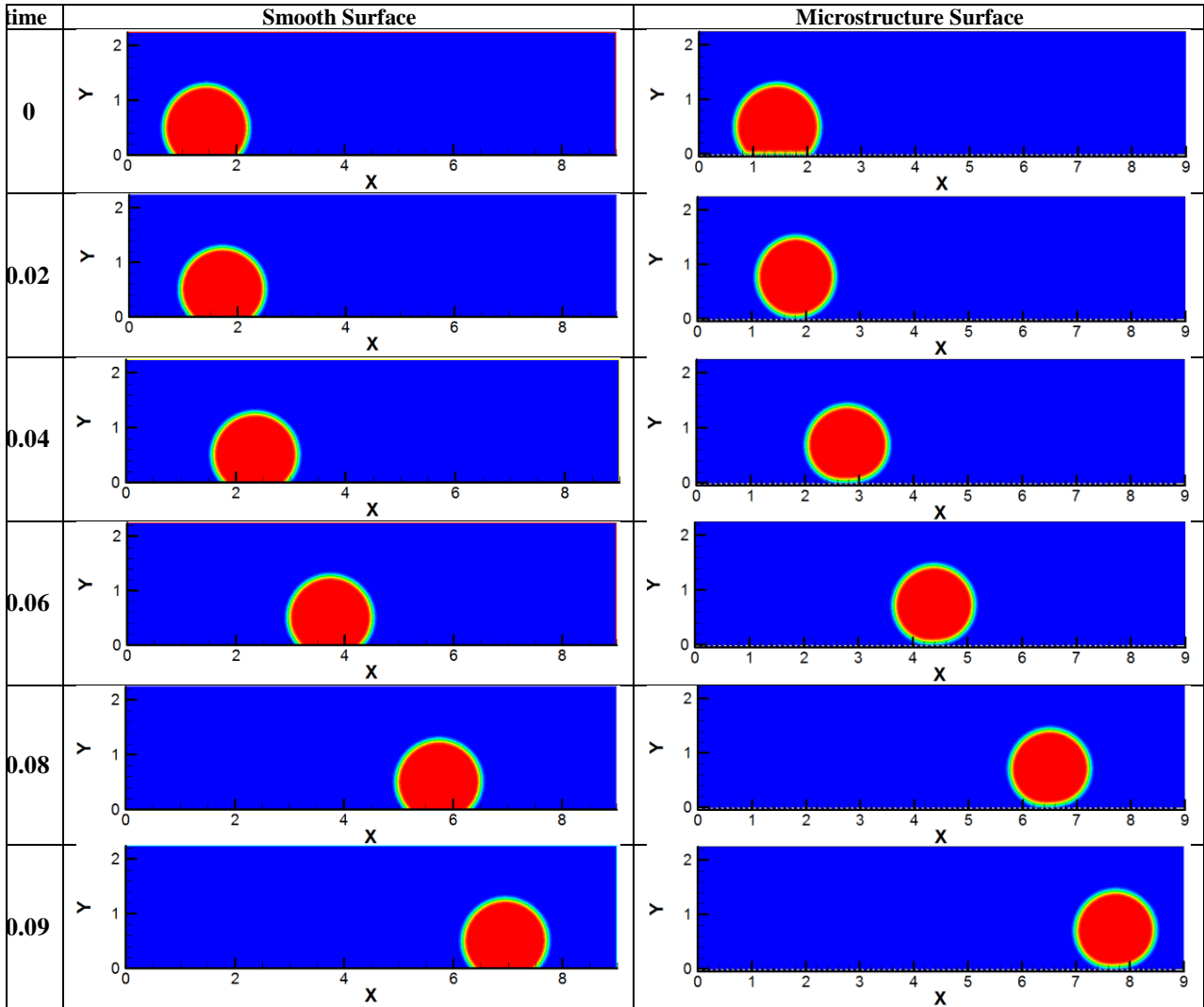


Fig 8: Comparison of the droplet motion on smoothed and microstructure surfaces at different times

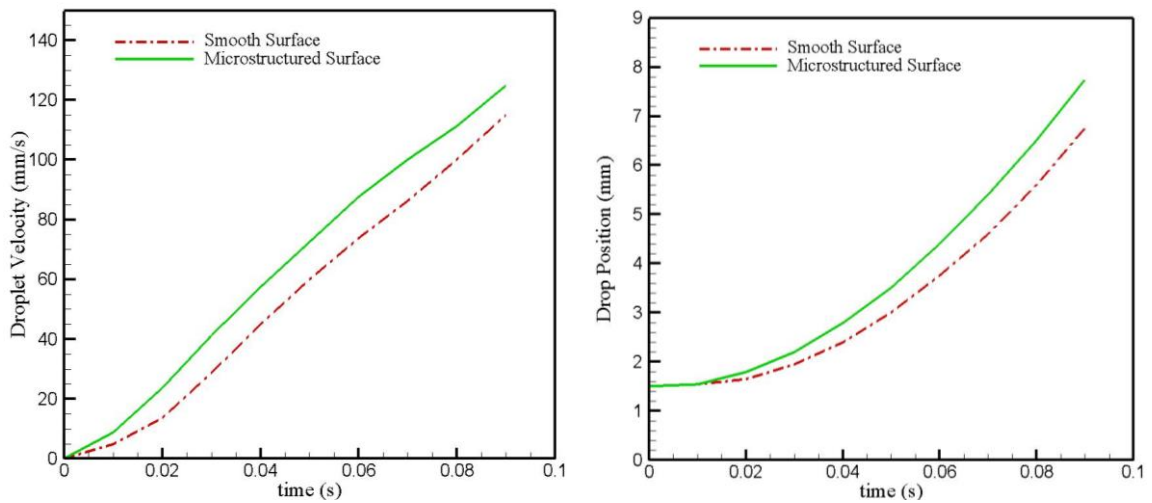


Fig. 9: Comparison of position and velocity of drop on inclined surface



## Acknowledgements

The authors would like to express special appreciation to the Aerospace Research Institute (ARI) and Max Planck Institute of Colloids and Interfaces for supporting this research

## Conflict of Interest

There is no conflict of interest by the authors.

## References

- [1] K. Manoharan and S. Bhattacharya, "Superhydrophobic surfaces review: Functional application, fabrication techniques and limitations", *Journal of Micromanufacturing*, vol. 2, no. 1, pp. 59–78, 2019.
- [2] S. Dey and B. Giri, "Iodine fact on human health and health problems: a review", *Med Clin Rev 2016*; vol.2, no. 1, pp. 1–6, 2016.
- [3] F.H. Rajab, Z. Liu and L. Li, "Long term superhydrophobic and hybrid superhydrophobic/superhydrophilic surfaces produced by laser surface micro/nano surface structuring", *Appl Surf Sci*, vol. 466, pp. 808–821, 2019.
- [4] P. Pou, J. Del Val, A. Riveiro, "Laser texturing of stainless steel under different processing atmospheres: from superhydrophilic to superhydrophobic surfaces", *Appl Surf Sci 2019*, vol. 475, pp. 896–905, 2019.
- [5] D. Huerta-Murillo, A. García-Girón, J.M. Romano, "Wettability modification of laser-fabricated hierarchical surface structures in Ti-6Al-4V titanium alloy," *Appl Surf Sci 2019*, vol. 463, pp. 838–846, 2019.
- [6] P. Wang, X. Qian and J. Shen, "Superhydrophobic coatings with edible biowaxes for reducing or eliminating liquid residues of foods and drinks in containers", *Bioresources 2018*, vol. 13, no. 1, pp. 1–2., 2018.
- [7] Z. Y. Deng, W. Wang, L. H. Mao, C. F. Wang and S. Chen, "Versatile Superhydrophobic and Photocatalytic Films Generated from TiO<sub>2</sub>-SiO<sub>2</sub> at PDMS and Their Applications on Fabrics", *J. Mater. Chem. A*, vol. 2, pp. 4178–4184, 2014.
- [8] L. F. Que, Z. Lan, W. X. Wu, J. H. Wu, J. M. Lin and M. L. Huang, "High-efficiency Dye-sensitized Solar Cells Based on Ultra-Long Single Crystalline Titanium Dioxide Nanowires", *J. Power Sources*, vol. 266, pp. 440–447, 2014.
- [9] Z. Liu, Y. Gou, J. Wang, and S. Cheng, "Frost Formation on a Super-hydrophobic Surface under Natural Convection Conditions", *International Journal of Heat and Mass Transfer*, vol. 51, pp. 5975–5982, 2008.
- [10] M. He, J. Wang, H. Li, X. Jin, J. Wang, B. Liu, and Y. Song, "Super-hydrophobic Film Retards Frost Formation", *Soft Matter*, vol. 6, pp. 2396–2399, 2010.
- [11] L. Mishchenko, B. Hatton, V. Bahadur, J. A. Taylor, T. Krupenkin, and J. Aizenberg, "Design of Ice-free Nanostructured Surfaces Based on Repulsion of Impacting Water Droplets", *ACS Nano*, vol. 4, pp. 7699–7707, 2010.
- [12] K. Javadi, S. H. Davoudian, "Surface Wettability Effect on the Rising of a Bubble Attached to a Vertical Wall", *IJMPF, Elsevier*, vol. 109, pp. 178-190, 2018.
- [13] T. Nishino, M. Meguro, K. Nakamae, M. Matsushita and Y. Ueda, "The Lowest Surface Free Energy Based on –CF<sub>3</sub> Alignment", *Langmuir*, vol. 15, pp. 4321–4323, 1999.
- [14] R. Kamali Moghadam, M. Taeibi Rahni, Kh. Javadi, S. Heyat Davoudian, R. Miller, "Influence of New Superhydrophobic Micro-structures on Delaying Ice Formation", *Colloids and Surfaces A: Physicochemical and Engineering Aspects*, vol. 595, 2020.
- [15] G. Zhu, J. Yao, L. Zhang, H. Sun, A. Li, and B. Shams, "Investigation of the Dynamic Contact Angle Using a Direct Numerical Simulation Method", *Langmuir*, vol. 32, pp. 1736–11744, 2016.
- [16] H. Jia, X. Xiao, Y. Kang, "Investigation of a free rising bubble with mass transfer by an arbitrary Lagrangian–Eulerian method", *International Journal of Heat and Mass Transfer*, vol. 137, pp. 545–557, 2019.
- [17] S. McKee, M. F. Tome, V. G. Ferreira, J. A. Cuminato, A. Castelo, F. S. Sousa, N. Mangiavacchi, "The MAC method", *Computers & Fluids*, vol. 37, pp. 907–930, 2008.
- [18] P. Yue, C. Zhou, J. J. Feng, C. F. Ollivier-Gooch, H. H. Hu, "Phase-field simulations of interfacial dynamics in viscoelastic fluids using finite elements with adaptive meshing", *J. Comput. Phys*, vol. 219, pp. 47–67, 2006.
- [19] M. van Sint Annaland, N. G. Deen, J. A. M. Kuipers, "Numerical simulation of gas bubbles behaviour using a three-dimensional volume of fluid method", *Chem. Eng. Sci.* vol. 60, pp. 2999–3011, 2005.
- [20] Y. Tanaka, Y. Washio, M. Yoshino, T. Hirata, "Numerical simulation of dynamic behavior of droplet on solid surface by the two-phase lattice Boltzmann method", *Computers & Fluids*, vol. 40, 68–78, 2011.
- [21] P. Tourkine, M. Le Merrer, and D. Quere, "Delayed Freezing on Water Repellent Materials", *Langmuir*, vol. 25, pp. 7214–7216, 2009.
- [22] G. Zhu, J. Yao, L. Zhang, H. Sun, A. Li, and B. Shams, "Investigation of the Dynamic Contact Angle Using a Direct Numerical Simulation Method", *Langmuir*, vol. 32, pp. 1736–11744, 2016.
- [23] R. Clift, J. R. Grace, and M. E. Weber, *Bubbles, Drops, and Particles*, Academic Press, 1978.
- [24] H-Y. Kim, H. J. Lee, and B. H. Kang, "Sliding of Liquid Drops Down an Inclined Solid Surface", *Journal of Colloid and Interface Science*, vol. 247, pp. 372–380, 2002.